

See discussions, stats, and author profiles for this publication at: <https://www.researchgate.net/publication/354637012>

Wave energy resource assessment at Hvide Sande on the west coast of Denmark

Conference Paper · September 2021

CITATIONS

0

READS

15

3 authors, including:



Irina Dolguntseva Temiz

Uppsala University

36 PUBLICATIONS 216 CITATIONS

[SEE PROFILE](#)



Tatiana Potapenko

Uppsala University

7 PUBLICATIONS 5 CITATIONS

[SEE PROFILE](#)

Some of the authors of this publication are also working on these related projects:



MariNET2 [View project](#)



DUAL Ports [View project](#)

Wave energy resource assessment at Hvide Sande on the west coast of Denmark

Irina Temiz*, Tatiana Potapenko, and Akash Vijay Kumar

Abstract—The wave power potential in the North Sea was studied in several publications for different locations. This paper estimates the wave power potential at a specific location, namely, near the town of Hvide Sande, located on the western coast of Denmark. To assess the wave energy resource at Hvide Sande, a hindcast model utilizing SWAN (Simulating WAVes Nearshore) simulation tool is developed. The model is calibrated and validated with the 8-years data from a wave measurement buoy located close to Hvide Sande. Significant wave heights from simulations show a high correlation with the buoy data, and the mean wave periods are in good agreement with the measurements. Utilizing 30-years ERA5 reanalysis wind and wave data provided by the European Centre for Medium-range Weather Forecasts, the model was used to obtain the sea states at four sites. These sites are chosen to fulfil the placement requirements of two wave energy converter concepts: Seabased and ECO Wave Power. The average annual power density is found from 17.3 kW/m to 18.32 kW/m for offshore locations and 10.8 kW/m for the breakwater location. The obtained results on wave power potential and the time series of sea states during the 30-years period will be used for the (micro-) grid studies for the town of Hvide Sande.

Index Terms—Model validation, seasonal variability, SWAN, wave energy, wave power density.

I. INTRODUCTION

THIS work has been done as a part of the “DUAL Ports” project, where a potential of grid integration of wave energy converters (WECs) and WEC arrays into the (micro-) grid of the port of Hvide Sande is studied. Hvide Sande is located at 56°N and 8.1°E on the western coast of Denmark, lying on the edge of the North Sea. Information on the wave climate and the wave energy potential in the area of interest is required for the project.

Wave energy potential in the North Sea was studied in several papers. In [1], the wave energy potential was presented for 31 different locations in the North Sea. The assessment was based on physical measurements and hindcasting models such as MIKE 21 OWS, WINCH model, UK Water Wave model. The available wave power density near shore at a distance less than 11 km was estimated at less than 11 kW/m. In [2], the wave energy potential was studied for one location in

the North Sea using MIKE 21 OWS hindcasting model. The site was chosen 100 km away from the coast, and the available wave energy density was 9.8 kW/m. However, these studies utilized models for deep and intermediate waters suitable for large areas but not applicable for near-shore analysis.

Wave climate nearby Hantsholm, located at the west coast of Denmark, was analysed in [3]. The long-term average wave power density was estimated at 7 kW/m. A long-term high-resolution database of wave energy potential for the North Sea was presented in [4]. The wave power density was assessed to be from 5 kW/m to more than 15 kW/m with the most energetic seas in the North East of the investigated region. These studies confirm that the Danish part of the North Sea has a good potential for wave energy. However, the North Sea did not receive sufficient attention from the wave energy development point of view since it was always perceived as having “low” wave power potential. Concerning the present study, it should be noted that the site of interest is not covered in [3] and [4].

Hence, the authors concluded that a detailed analysis of the wave climate nearby Hvide Sande is needed. Simulating WAVes Nearshore (SWAN) model [5], [6] is used to obtain long-term (30 years) wave spectral data. The hindcast data are validated against the measurements done in proximity to the port of Hvide Sande. The paper is partly based on results presented in [7].

II. WAVE MODEL

In this study, the SWAN model available within the Delft3D-WAVE module v. 3.05 [8] is applied. SWAN is the third generation discrete spectral wave model that describes the evolution of the wave energy spectrum in two-dimensional models under the arbitrary wind, currents, and bathymetry conditions [6].

The evolution of wave spectrum is described by the balance equation of the two-dimensional action density spectrum $N(\sigma, \theta)$, given in Cartesian coordinates as in (1).

$$\frac{\partial N}{\partial t} + \frac{\partial c_x N}{\partial x} + \frac{\partial c_y N}{\partial y} + \frac{\partial c_\sigma N}{\partial \sigma} + \frac{\partial c_\theta N}{\partial \theta} = \frac{S}{\sigma} \quad (1)$$

where σ is the angular frequency as observed in a reference frame moving with current velocity; θ is the wave propagation direction; $c = (c_x, c_y, c_\sigma, c_\theta)$ is the action propagation velocity in (x, y, σ, θ) space; and $S = S(\sigma, \theta, x, y, t)$ is the net sink and source term representing the effects of generation, dissipation, and

The ID number of paper submission is 2235 and the conference track is WRC.

This work was supported in part by the “DUAL Ports” project co-financed by the European Union under the European Regional Development Fund (ERDF) within the Interreg North Sea Region Programme 2015-2020 and Swedish Energy Agency (PA No. 48346-1), STandUP for Energy, ÅForsk (17-550) and Uppsala University.

I. Temiz, T. Potapenko and A. V. Kumar are all with the Division of Electricity, Department of Electrical Engineering, Uppsala University, Box 65, 75103 Uppsala, Sweden.

*Corresponding author: irina.temiz@angstrom.uu.se.

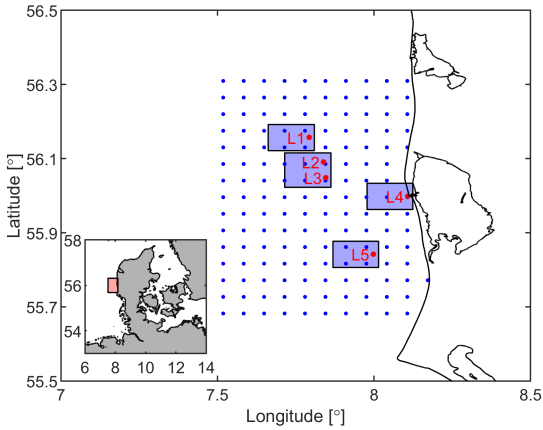


Fig. 1. The model area is located outside the west coast of Denmark. The blue dots denote the coarse grid nodes. The red dots denote the SWAN output locations. The blue rectangles are nested grid areas of the output locations.

nonlinear wave-wave interactions [5]. The action density spectrum $N(\sigma, \theta)$ is related to the energy density spectrum $E(\sigma, \theta)$ via $N(\sigma, \theta) = E(\sigma, \theta)/\sigma$.

In total, six terms are contributing to the sink and source terms:

$$S = S_{in} + S_{ds,w} + S_{ds,b} + S_{ds,br} + S_{nl3} + S_{nl4} \quad (2)$$

where S_{in} is the wave growth due to the wind; $S_{ds,w}$, $S_{ds,b}$ and $S_{ds,br}$ denote wave decay due to whitecapping, bottom friction and depth induced wave breaking respectively; and S_{nl3} and S_{nl4} are the nonlinear transfer of wave energy through three-wave and four-wave interactions.

A. Wind input

The transfer of wind energy to waves is described in SWAN [9] by:

$$S_{in}(\sigma, \theta) = A + BE(\sigma, \theta) \quad (3)$$

where A and B describe linear and exponential growth by the wind. The linear growth term A is based on the expression from [10] with an added filter [11] to reduce wave growth at frequencies lower than the Pierson-Moskowitz frequency [12]. The exponential growth term B follows the expression given in [13]. Explicit formulas for A and B can be found in [9].

B. Dissipation

Dissipation of wave energy depends on whitecapping, bottom friction and depth-induced wave breaking.

1) *Whitecapping*: The whitecapping is represented by the pulse-based model of [14], that is, in terms of wavenumber [15], given by:

$$S_{ds,w} = -\Gamma \tilde{\sigma} \frac{k}{k} E(\sigma, \theta) \quad (4)$$

where the coefficient Γ depends on the overall wave steepness, $\tilde{\sigma}$ and \tilde{k} are the mean frequency and the mean wavenumber, respectively. Since the wind input

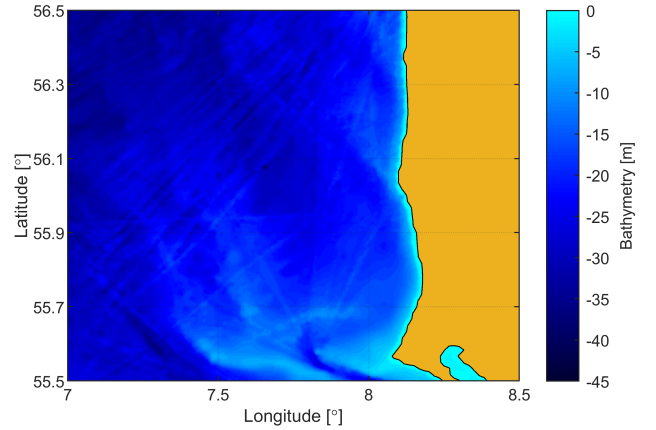


Fig. 2. The bathymetry map of the model area.

model by [13] is used, the same model is chosen for whitecapping in Delft-3D with the default settings provided since SWAN v. 40.91A [9].

2) *Bottom friction*: The bottom friction models [16]–[18] can all be expressed in the following form [9]:

$$S_{ds,b} = -C_b \frac{\sigma^2}{g^2 \sinh^2 kd} E(\sigma, \theta) \quad (5)$$

where C_b is a bottom friction coefficient and d is the depth. Following suggestion given in [19] for the depth-limited wind-sea conditions in the North Sea, the JONSWAP empirical model [16] with the recommended in Delft-3D bottom friction coefficient $C_b = 0.067 \text{ m}^2/\text{s}^3$ is used here.

3) *Depth-induced wave breaking*: The process of depth-induced wave breaking is described by a spectral version [20] of the bore model [21], which is expressed in SWAN as:

$$S_{ds,br} = -\frac{D_{tot}}{E_{tot}} E(\sigma, \theta) \quad (6)$$

where E_{tot} and D_{tot} is the rate of dissipation of the total energy due to wave breaking. The default settings of SWAN given in Delft-3D are used in the model.

C. Nonlinear wave-wave interaction

Nonlinear wave-to-wave interactions refer to so-called quadruplets, i.e., four-wave interactions typical for intermediate and deep water, and triads, i.e., three-wave interactions observed in shallow water. Both quadruplets and triads transfer wave energy from the spectral peak to lower and higher frequencies leading to the evolution of the wave spectrum. In SWAN, quadruples and triads are computed using the discrete interaction approximation [22] and the lumped triad approximation [23], respectively. Only quadruplets are enabled in the model since activating of the triads does not improve the results but increases the computational time.

III. MODEL SET-UP

The model covers the area of 7.5 to 8.15 degrees east and 55.7 to 56.3 degrees north. The coarse grid with a resolution of $4 \text{ km} \times 5 \text{ km}$ is shown in Fig. 1.

TABLE I
THE SWAN OUTPUT LOCATIONS.

	Coordinates	Distance from harbour (km)	Depth (m)
L1	56°9'25.85"N 7°47'34.55"E	26	30.3
L2	56°5'26.79"N 7°50'18.74"E	20	27.3
L3	56°2'54.71"N 7°50'45.13"E	17	27.5
L4	55°59'54.5"N 8°6'29.20"E	1	6.5
L5	55°50'31.8"N 7°59'52.2"E	19	19.5

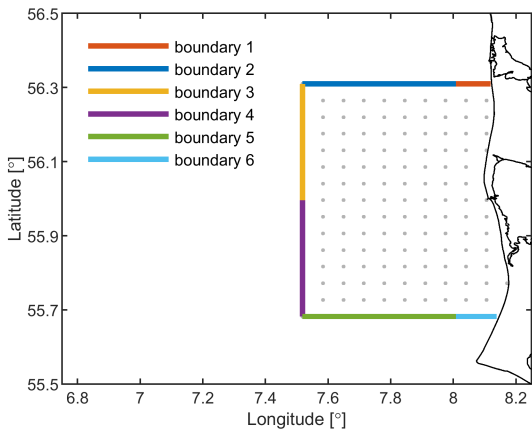


Fig. 3. The domain open boundaries. Space-time varying boundary conditions are defined separately along each boundary 1–6.

Nested grids sized 9 km × 8 km at the the SWAN output locations given in Table I have a resolution of 500 m × 500 m. Locations L1–L4 are chosen as potential placements of wave power plants, and the wave measurement buoy is placed at location L5.

The bathymetry for the model shown in Fig. 2 is constructed from the GEBCO a 15 arc-second gridded bathymetry database [24], and the coastline data from the latest Global Self-consistent, Hierarchical, High-resolution Geography Database (GSHHG) [25].

The ERA5 reanalysis wind and wave datasets by the European Centre for Medium-range Weather Forecasts (ECMWF) are utilized [26]. The wind and wave data have an hourly temporal resolution. The period for the past 30 years from 1990 to 2019 is considered.

The wind boundary conditions, namely, the average wind speed at a 10 m height and wind direction given in the nautical convention, are implemented in the model. The wave boundary conditions include the significant height of wind waves, the mean wave period and the mean wave direction. The wind and wave boundary conditions are space-time varying, where the domain open boundaries are divided as shown in Fig. 3. The calibration of different wind-wave generation/propagation models and boundary conditions available in Delft-3D were investigated in [7].

IV. MODEL VALIDATION

A. Buoy data

The buoy measurement data were recorded from February 10, 2005, to December 31, 2012, by a wave

rider buoy located at 55°50'31.8"N and 7°59'52.2"E (location L5), just off the south-western coast of Hvide Sande. The water depth at the buoy location is 19.5 m. The wave datasets contain the sea state statistical parameters: the significant wave height H_{m0} , maximum wave height H_{max} , wave direction, and the mean wave period T_{01} . However, some time intervals in the measurements are missing. In total, 46951 buoy measurements are available with a data availability of 68.51%.

Before using the buoy measurement data, the dataset was processed and subject to quality control tests to verify the validity and reliability of the data. First, the outliers and data outside physically realistic limits were removed. Then, the wave parameters were averaged using a one-hour moving average. The one-hour time window was selected to compare the model output data obtained based on the input data of hourly temporal resolution. Finally, the data were interpolated on regularly spaced 30-minutes time vectors to make the measurement data suitable for comparison with the modelled data.

B. Statistical parameters

The model results are compared with the buoy measurement data. Several indices are used for the modelled data assessment: Pearson's correlation coefficient (R) given in (7), the root-mean-square error ($RMSE$) defined by (8), the scatter index (SI) given in (9), and the bias ($Bias$) in (10).

$$R = \frac{\sum_{i=1}^N (x_i - \bar{x})(y_i - \bar{y})}{\sqrt{\sum_{i=1}^N (x_i - \bar{x})^2 \sum_{i=1}^N (y_i - \bar{y})^2}}, \quad (7)$$

$$RMSE = \sqrt{\frac{1}{N} \sum_{i=1}^N (x_i - y_i)^2}, \quad (8)$$

$$SI = \frac{RMSE}{\bar{y}}, \quad (9)$$

$$Bias = \bar{x} - \bar{y}, \quad (10)$$

where x_i stands for the modelled data points and y_i for the observed data from the wave measurement buoy; \bar{x} and \bar{y} are the average values of the modelled and observed data sets, respectively; N is the number of data points in both data sets.

The statistical results of validation of the significant wave height H_{m0} and the mean wave period T_{01} are presented in Table II and Table III, respectively.

The significant wave height H_{m0} shows a high Pearson's correlation coefficient R equal to 95.95% for the entire time period, the bias is negligible, and the $RMSE$ is limited by 0.24 m. The overall scatter index SI is limited by 17.73% showing a strong agreement.

The mean wave period T_{01} shows a good agreement but with a reduced correlation compared to H_{m0} varying from 79.60% to 87.23% through the years and equal to 84.38% for the entire period. T_{m01} has a negative bias of -0.38 s for the whole period indicating that the hindcast mean wave period is slightly underestimated.

TABLE II
VALIDATION H_{m0} .

	R	$RMSE$ (m)	SI	$Bias$ (m)
2005	94.44%	0.24	18.01%	-0.01
2006	96.10%	0.23	16.71%	0.03
2007	96.75%	0.24	16.69%	-0.03
2008	96.26%	0.23	18.75%	-0.003
2009	95.47%	0.23	17.68%	-0.01
2010	93.69%	0.23	20.30%	-0.001
2011	96.90%	0.22	16.28%	0.04
2012	96.43%	0.23	16.86%	0.02
<i>Total</i>	<i>95.95%</i>	<i>0.23</i>	<i>17.73%</i>	<i>0.004</i>

TABLE III
VALIDATION T_{01} .

	R	$RMSE$ (s)	SI	$Bias$ (s)
2005	81.66%	0.70	15.85%	-0.37
2006	84.14%	0.70	15.86%	-0.40
2007	85.75%	0.76	17.11%	-0.42
2008	87.23%	0.78	18.15%	-0.42
2009	87.23%	0.62	14.86%	-0.34
2010	79.60%	0.74	18.07%	-0.43
2011	82.74%	0.73	16.60%	-0.32
2012	86.21%	0.68	15.59%	-0.32
<i>Total</i>	<i>84.38%</i>	<i>0.72</i>	<i>16.69%</i>	<i>-0.38</i>

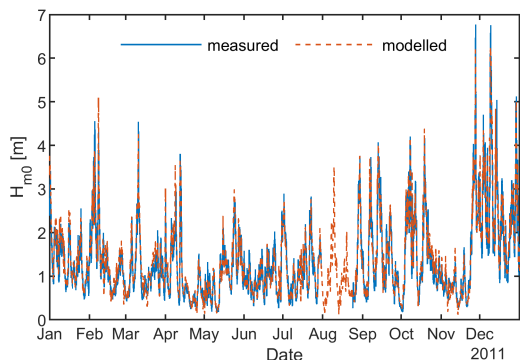


Fig. 4. Time series comparison of computed and measured data for significant wave height.

The overall scatter index of T_{01} is 16.69%, showing a strong agreement between the modelled and measured data.

C. Time series data

Comparison examples of time series data from 2011 are shown in Figs. 4–6, where simulated and the measured data of the significant wave height, mean wave period and mean wave direction are shown. In Fig. 4, it can be observed that the modelled data slightly underestimates large values of H_{m0} . It implies that an additional model to predict the extreme wave heights should be used. The mean wave periods predicted by the model are less than the measured values (Fig. 5), and the difference becomes noticeable for short wave periods. It can also be noted that very large (greater than 15 s) mean wave periods occurred during Febru-

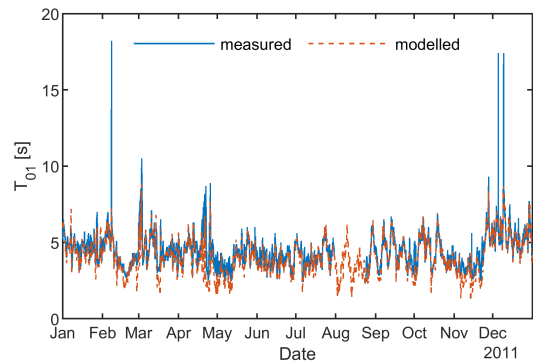


Fig. 5. Time series comparison of computed and measured data for mean wave period.

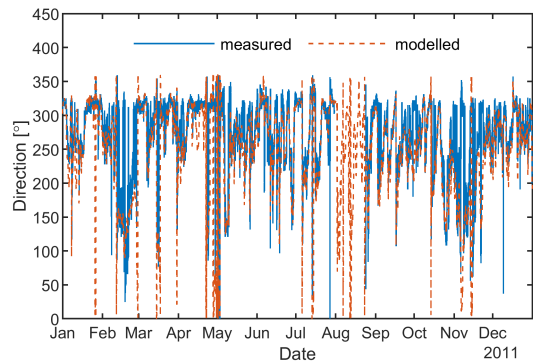


Fig. 6. Time series comparison of computed and measured data for mean wave direction. Directions are given according to the nautical convention.

ary and December 2011 and were not captured by the model. However, the long mean wave periods continue for a short time of 2–2.5 hours and were possibly caused by storms with rapid wind speed growth and changed wind direction (see Fig. 6).

V. RESULTS

The locations of interest are selected as potential placement of wave power plants. Locations L1–L3 are considered for an underwater WEC, e.g., developed by Seabased [27]. These locations are chosen so that the distance to the locations does not exceed 30 km; there exists relatively flat seabed area sufficient for installation of 2–10 MW wave power park, and the depth at the site is greater than or equal to 25 m. Location L4 is chosen very close to the breakwater nearby the entrance to the harbour of Hvide Sande. It is considered for potential placement of a smaller breakwater-integrated WEC, e.g., developed by ECO Wave Power [28].

The average, standard deviation and maximum wave power density at the four locations calculated for the 30-years period are presented in Table IV. Figs. 7 and 8 illustrate the average wave power variations through the 30-years period and the intra-annual variations, respectively. The wave power density of a sea state available per meter of the wave crest is calculated according to formula (11).

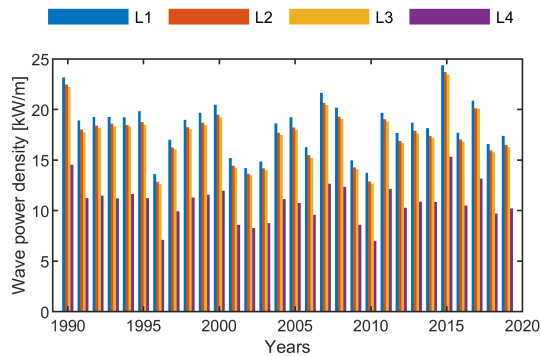


Fig. 7. Average annual wave power density calculated for locations L1–L4 over a period of 30 years.

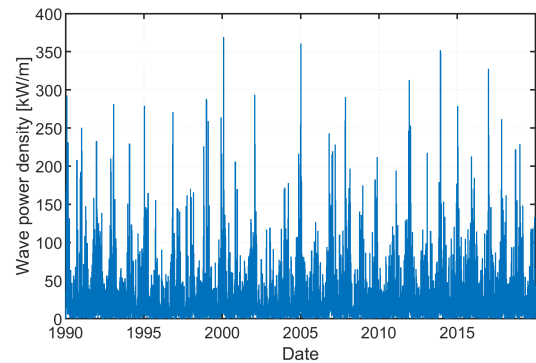


Fig. 9. Wave power density at location L1 plotted for the 30-years period.

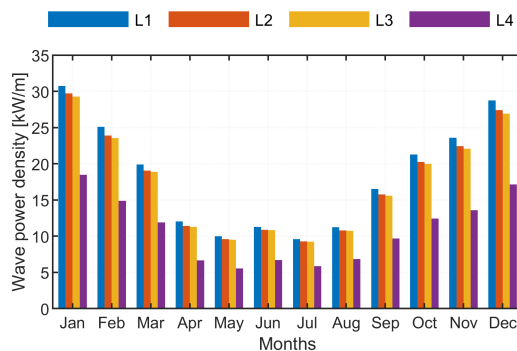


Fig. 8. Intra-annual variation of the wave power density calculated for location L1–L4 over a period of 30 years.

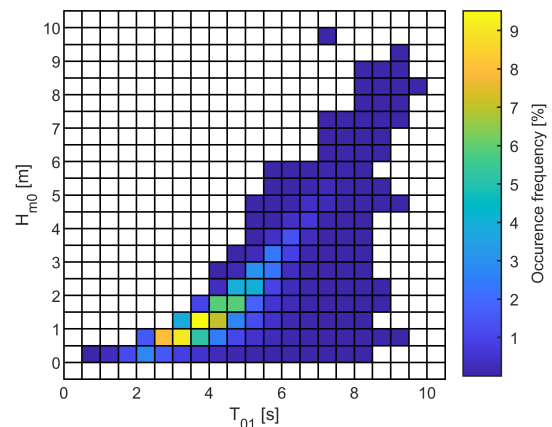


Fig. 10. Scatter diagram of the wave climate at L1 obtained for the 30-years period.

TABLE IV
AVERAGE WAVE POWER DENSITY AND ITS STANDARD DEVIATION FOR LOCATIONS L1–L4.

Location	P_{avg} (kW/m)	P_{std} (kW/m)	P_{max} (kW/m)
L1	18.32	23.06	369.20
L2	17.52	22.34	365.76
L3	17.30	22.20	369.26
L4	10.80	14.66	162.25

$$P = \frac{\rho g^2 H_{m0}^2 T_{01}}{64\pi}, \quad (11)$$

where ρ is the seawater density, and g is the gravitational acceleration.

The average wave power densities at locations L1, L2 and L3 are similar but slightly increasing for the areas located farther offshore. Although the average wave power density available at L4 is lesser due to various wave energy dissipation mechanisms described above, the wave power potential at L4 can still be overestimated by the model due to the proximity of the coastline and the presence of the breakwater.

Figs. 9 and 10 illustrate the wave power density at location L1 as a time series, and a scatter diagram of sea states and their occurrence frequency, respectively. It can be observed that the most frequent sea states occur at milder sea states with significant wave heights not greater than 3 m/s and mean wave periods up to 7 s and therefore carry less wave energy. However,

extreme sea states with a significant wave height up to 10 m may occur at L1, resulting in a very large values of wave power density in Fig. 9. It also explains a large wave power density variability illustrated by the standard deviations and maxima in Table IV.

Figs. 11 and 12 show directional wave power density variation for location L1. Directional wave power density variations for the other locations are similar. In Fig. 11, only a wave power density of maximum 50 kW/m is plotted, and the occurrence of higher wave power density sea states with respect to wave direction is illustrated in Fig. 12. It can be noted that the majority of waves come from the north-westerly direction, and fewer waves are from westerly and south-westerly directions. The most energetic waves also come from these directions. Sea states corresponding to a wave power density greater than 50 kW/m are considered extreme for both wave energy technologies.

VI. DISCUSSION

The wave power density of the North Sea was estimated for different locations and using various methods in earlier publications. For example, in [2] the wave energy density available at the site in the North Sea 100 km away from the coast was estimated at 9.8 kW/m. Considering offshore location of the site, its wave power density is underestimated compared to

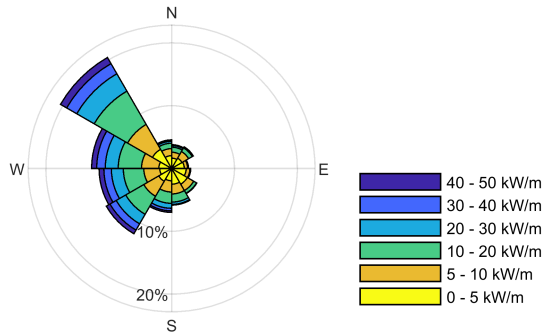


Fig. 11. Wave rose for wave power density at location L1 obtained for the 30-years period. Only sea states with wave power density less than or equal to 50 kW/m are plotted.

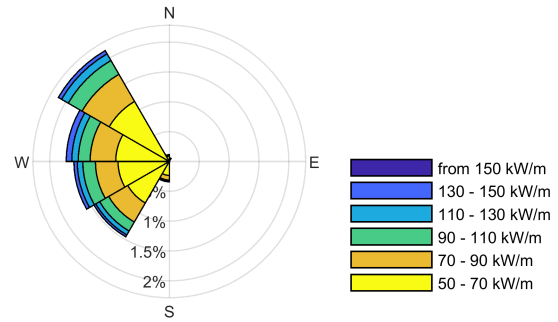


Fig. 12. Wave rose for wave power density at location L1 obtained for the 30-years period. Only sea states with wave power density greater than 50 kW/m are plotted.

the obtained power potential in this paper. A relatively low wave power density was presented in [3], which could be the result of the site location, depth and the time interval of hindcasting. Wave power potential presented in [4] agrees well with the present model results.

Comparing results from [1] with the wave power density at locations L3 (17 km from shore) and L4 (1 km from shore), it can be noted that the wave power potential estimated for locations L4 is overestimated and for locations very close to shore different models should be used, e.g., SWASH [29]. On the other hand, the estimated wave power potential of 11 kW/m [1] is also an average value calculated over the entire North Sea. Therefore the wave power potential at a particular location nearby Hvide Sande may be different. Nevertheless, the wave power potential at location L4 should be used with caution since it may provide overestimated output power values from a WEC.

In [30] the wave power potential of the North Sea was between 12–17 kW/m, which seems the closest to the potential predicted by the model presented in this paper. Sørensen and Fernández Chozas [30] used the estimated wave power potential to find an annual energy production of 77 TWh employing the Wave Dragon conversion technology in the transnational grid cooperation approach. This work aims to estimate the wave power production at Hvide Sande using different technologies. Wave power plants by Seabased and ECO Wave Power are designed to operate in mild to moderate sea conditions in intermediate water depths (Seabased) or on breakwaters (ECO Wave Power). Therefore, these technologies can be well suited to the wave climate of Hvide Sande. Nevertheless, rare storms (see Fig. 12) shall be accounted for in the WEC design.

VII. CONCLUSION

Wave power potential at the proximity of the Danish town of Hvide Sande was estimated and presented in this paper. The assessment was done for four different locations, which were chosen to suit at least two different wave energy technologies. The results showed

that the available average wave power potential varies from approximately 11 kW/m to 18 kW/m. However, a relatively mild wave climate brings challenges of large wave power variability through the lifetime of a WEC as well as rare but extreme sea states, which the wave energy device should survive.

The hindcast data of sea states presented in the paper were obtained using a SWAN model calibrated and validated against 8-years buoy measurement data recorded nearby Hvide Sande. The simulations showed a very good of the significant wave heights and a good agreement of the mean wave energy periods.

In the future, detailed information about the sea states at Hvide Sande will be used to estimate the economic potential of wave energy to contribute to renewable electricity production at this site.

REFERENCES

- [1] C. Beels, J. C. C. Henriques, J. D. Rouck, M. T. Pontes, G. D. Backer, and H. Verhaeghe, "Wave Energy Resource in the North Sea," *7th European Wave and Tidal Energy Conference*, p. 10, 2007.
- [2] U. Henfridsson *et al.*, "Wave energy potential in the Baltic Sea and the Danish part of the North Sea, with reflections on the Skagerrak," *Renewable Energy*, vol. 32, no. 12, pp. 2069–2084, 2007.
- [3] J. Fernández-Chozas, N. Helstrup Jensen, H. Sørensen, J. Kofoed, and A. Kabuth, "Predictability of the power output of three wave energy technologies in the Danish North Sea," *International Journal of Marine Energy*, vol. 1, pp. 84–98, apr 2013.
- [4] G. Lavidas and H. Polinder, "North Sea Wave Database (NSWD) and the Need for Reliable Resource Data: A 38 Year Database for Metocean and Wave Energy Assessments," *Atmosphere*, vol. 10, no. 9, p. 551, sep 2019.
- [5] N. Booij, R. C. Ris, and L. H. Holthuijsen, "A third-generation wave model for coastal regions: 1. Model description and validation," *Journal of Geophysical Research: Oceans*, vol. 104, no. C4, pp. 7649–7666, apr 1999.
- [6] R. C. Ris, L. H. Holthuijsen, and N. Booij, "A third-generation wave model for coastal regions: 2. Verification," *Journal of Geophysical Research: Oceans*, vol. 104, no. C4, pp. 7667–7681, apr 1999.
- [7] A. Vijay Kumar, "Wave resource assessment using numerical wave modelling," Master's thesis, Uppsala University, Department of Electrical Engineering, 2020.
- [8] Deltares systems, *Delft3D-WAVE. Simulation of short-crested waves with SWAN. User manual*, 2020.
- [9] SWAN, *Scientific and technical documentation*. Delft: Delft University of Technology, Environmental Fluid Mechanics Section, 2020.

- [10] L. Cavaleri and P. M. Rizzoli, "Wind wave prediction in shallow water: Theory and applications," *Journal of Geophysical Research*, vol. 86, no. C11, pp. 10,961–10,973, 1981.
- [11] H. L. Tolman, "Effects of Numerics on the Physics in a Third-Generation Wind-Wave Model," *Journal of Physical Oceanography*, vol. 22, no. 10, pp. 1095–1111, oct 1992.
- [12] W. J. J. Pierson and L. Moskowitz, "A Proposed Spectral Form for Fully Developed Wind Seas Based on the Similarity Theory of S. A. Kitaigorodskii," *Journal of Geophysical Research*, vol. 69, no. 24, pp. 5181–5190, 1964.
- [13] G. J. Komen, S. Hasselmann, and K. Hasselmann, "On the Existence of a Fully Developed Wind-Sea Spectrum," *Journal of Physical Oceanography*, vol. 14, no. 8, pp. 1271–1285, 1984.
- [14] K. Hasselmann, "On the spectral dissipation of ocean waves due to white capping," *Boundary-Layer Meteorology*, vol. 6, no. 1-2, pp. 107–127, mar 1974.
- [15] Wamdi Group, "The WAM Model—A Third Generation Ocean Wave Prediction Model," *Journal of Physical Oceanography*, vol. 18, no. 12, pp. 1775–1810, dec 1988.
- [16] K. Hasselmann *et al.*, "Measurements of Wind-Wave Growth and Swell Decay during the Joint North Sea Wave Project (JONSWAP)," Tech. Rep. 12, 1973.
- [17] J. I. Collins, "Prediction of shallow-water spectra," *Journal of Geophysical Research*, vol. 77, no. 15, pp. 2693–2707, may 1972.
- [18] O. S. Madsen, Y.-K. Poon, and H. C. Graber, "Spectral Wave Attenuation by Bottom Friction: Theory," in *21st International Conference on Coastal Engineering*. Costa del Sol-Malaga, Spain: American Society of Civil Engineers, 1988, pp. 492–504.
- [19] E. Bouws and G. J. Komen, "On the Balance Between Growth and Dissipation in an Extreme Depth-Limited Wind-Sea in the Southern North Sea," *Journal of Physical Oceanography*, vol. 13, no. 9, pp. 1653–1658, sep 1983.
- [20] Y. Eldeberky and J. A. Battjes, "Parameterization of triad interaction in wave energy model," in *Proc. Coastal Dynamics Conf. Gdansk, Poland, 1995*, 1995, pp. 140–148.
- [21] J. A. Battjes and J. P. F. M. Janssen, "Energy Loss and Set-Up Due to Breaking of Random Waves," in *16th International Conference on Coastal Engineering*, Hamburg, Germany, 1978, pp. 569–587.
- [22] S. Hasselmann, K. Hasselmann, J. H. Allender, and T. P. Barnett, "Computations and Parameterizations of the Nonlinear Energy Transfer in a Gravity-Wave Spectrum. Part II: Parameterizations of the Nonlinear Energy Transfer for Application in Wave Models," *Journal of Physical Oceanography*, vol. 15, no. 11, pp. 1378–1391, nov 1985.
- [23] Y. Eldeberky and J. A. Battjes, "Spectral modeling of wave breaking: Application to Boussinesq equations," *Journal of Geophysical Research C: Oceans*, vol. 101, no. C1, pp. 1253–1264, 1996.
- [24] GEBCO Bathymetric Compilation Group 2020, "The GEBCO_2020 Grid – a continuous terrain model of the global oceans and land." UK, 2020.
- [25] P. Wessel and W. H. F. Smith, "A global, self-consistent, hierarchical, high-resolution shoreline database," *Journal of Geophysical Research: Solid Earth*, vol. 101, no. B4, pp. 8741–8743, apr 1996.
- [26] H. Hersbach *et al.*, "ERA5 hourly data on single levels from 1979 to present." 2018.
- [27] "Seabased." [Online]. Available: seabased.com
- [28] "Eco Wave Power." [Online]. Available: ecowavepower.com
- [29] SWASH, "User manual," Delft University of Technology, Environmental Fluid Mechanics Section, Delft, Tech. Rep., 2020.
- [30] H. C. Sørensen and J. Fernández Chozas, "The Potential for Wave Energy in the North Sea," in *3rd International Conference and Exhibition on Ocean Energy*, Bilbao, Spain, 2010, pp. 1–6.